Two-dimensional intrinsic ferromagnetic monolayer transition metal oxyhydroxide

Hongyu Chen [1], Peizhe Tang [2,3,*] and Jia Li [1,4,†]

[1] *Institute of Materials Research, Tsinghua Shenzhen International Graduate School, Tsinghua University, Shenzhen 518055, China*

[2] *School of Materials Science and Engineering, Beihang University, Beijing 100191, China*

[3] *Max Planck Institute for the Structure and Dynamics of Matter, Center for Free Electron Laser Science, 22761 Hamburg, Germany*

[4] *Guangdong Provincial Key Laboratory of Thermal Management Engineering and Materials, Tsinghua Shenzhen International Graduate School, Tsinghua University, Shenzhen 518055, China*

(Received 18 January 2021; revised 21 April 2021; accepted 22 April 2021; published 4 May 2021)

Using density functional theory within the generalized gradient approximation, we predict that monolayer vanadium oxyhydroxide (VOOH) and chromium oxyhydroxide (CrOOH) are two-dimensional (2D) ferromagnetic semiconductors. These two kinds of oxyhydroxides possess excellent thermal and dynamical stability as the free-standing 2D monolayer films. Our results show that the monolayer VOOH and CrOOH remain ferromagnetic ordering with the critical temperature up to ∼100 K, and the ferromagnetic ordering is due to a superexchange interaction in the near-90° V(Cr)-O-V(Cr) bonds in monolayer VOOH(CrOOH). However, the different occupancy of *d* electrons between the V^{3+} and Cr^{3+} ions gives rise to the different axes or planes of easy magnetization and the different magnetic anisotropy energies between the monolayer VOOH and CrOOH. Our study demonstrates that monolayer transition metal oxyhydroxides could be one category of testing ground for the investigation of 2D ferromagnets.

DOI: 10.1103/PhysRevB.103.195402

I. INTRODUCTION

Layered two-dimensional (2D) magnetic materials have attracted much attention in recent years because of their potential application as the essential elements in layered spintronic devices [1–4]. Meanwhile, many exotic phenomena, such as quantum anomalous Hall effect [5–7], skyrmions [8–11], and magneto-optical effect [12–14] in these 2D systems have been successfully predicted and observed. According to the Mermin-Wagner theorem [15], the long-range magnetic ordering cannot survive in 2D materials with the isotropic magnetic property at finite temperature. However, the magnetic anisotropy can break this restriction and induce the long-range magnetic ordering. For example, few-layer $Cr_2Ge_2Te_6$ film is advocated as a 2D Heisenberg ferromagnet with considerable magnetic anisotropic energy (MAE) [16], even-layer CrI_3 film is demonstrated to be a 2D A-type interlayer antiferromagnet with a large band gap [17], and Fe_3GeTe_2 thin film is shown to be a metallic ferromagnet [18]. Moreover, magnetic properties in these 2D materials can be manipulated by external fields [19–22]. In bilayer CrI_3, the electrostatic doping can lead to a transition from an antiferromagnetic (AFM) to an ferromagnetic (FM) ground state without the magnetic field [23]. For the FM semiconductor $Cr_2Ge_2Te_6$, the critical temperature T_c modulation is achieved by applying hydrostatic pressure [24], and the electric current is theoretically demonstrated to induce an easy-plane magnetic anisotropy in Fe_3GeTe_2 by spin-orbit torque [25]. Simultaneously, 2D magnetic materials are still desirable to be explored for more intriguing phenomena and applications.

Transition metal oxyhydroxides (TMOOHs) are widely applied in electrocatalysis [26–28], and their spin states and magnetic moments located at the transition metal atoms are regarded to impact the charge transfer in the process of catalysis [29]. Inspired by this, the degree associated with their magnetic properties, such as spin or magnetic moment, can be modulated by an external field, applying to the spintronics. Moreover, TMOOHs possess layered structures [30–32], which means that they may exist as free-standing monolayers to be used in low-dimensional devices. In addition, ultrathin FeOOH nanosheets have been successfully synthesized from the intermediate of ferrous hydroxide [$Fe(OH)_2$] nanosheets, showing to be a room-temperature FM semiconductor [32] and monolayer FeOOH was theoretically predicted to be stable and possess AFM ground state [33]. Meanwhile, the CoOOH and CrOOH layered materials with the triangular lattice of cation have been synthesized long before and were demonstrated to have similar layered structures to the FeOOH [32]. In this regard, we expect to demonstrate a series of stable two-dimensional materials with intrinsic magnetism from this kind of materials.

In this paper, by using first-principles calculations, we investigate the structural and magnetic behaviors of a series of monolayer TMOOHs (TM = V, Cr, Mn, Co, Ni), whose prototype is the 2D magnet of FeOOH with layered structure [33]. We indeed find that VOOH and CrOOH are two new stable 2D magnets with long-range FM ordering whose structural stabilities confirmed by phonon spectra and first-principles molecular dynamics (FPMD) simulations. And the long-range FM ordering originates from the superexchange

*peizhet@buaa.edu.cn
†li.jia@sz.tsinghua.edu.cn

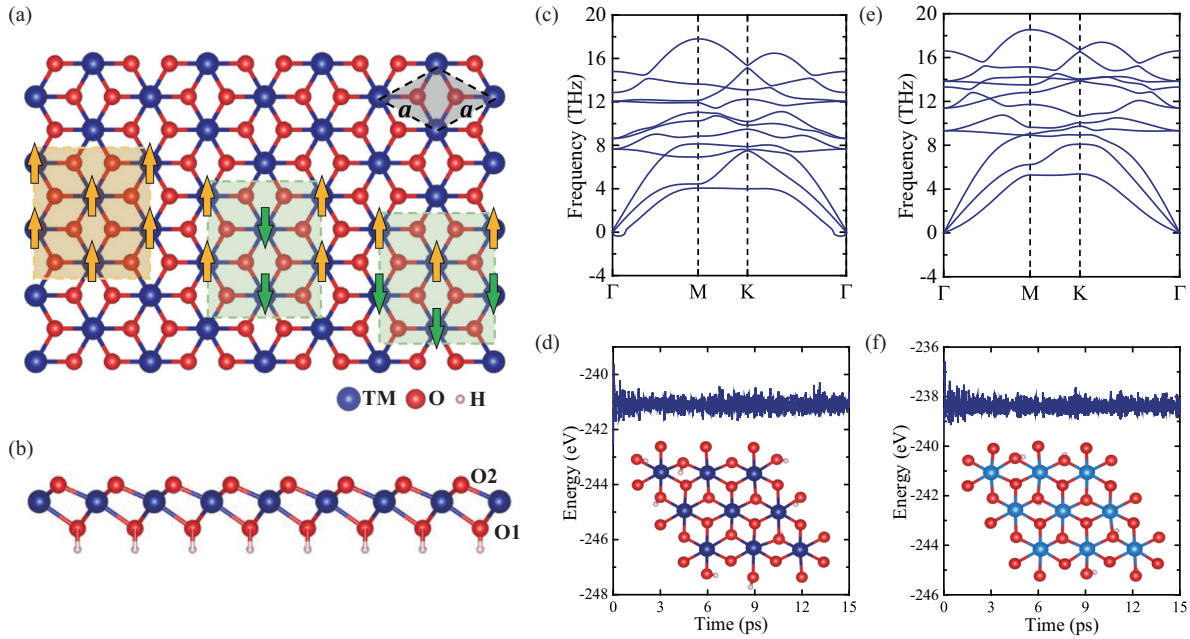

FIG. 1. (a) Top and (b) side views of the monolayer TMOOH with transition metal atoms represented by blue balls, O atoms represented by red balls, and H atoms represented by pink balls. The rhombic unit cell is marked by the black dashed lines. And the FM and AFM configurations (the stripe AFM and the zigzag AFM configurations) constructed in $2 \times 2 \times 1$ supercells are marked by yellow and green dashed rectangular boxes, respectively. Calculated phonon spectra for the monolayer (c) VOOH and (e) CrOOH. Evolutions of total energies during FPMD simulations for monolayer (d) VOOH and (f) CrOOH at the temperature of 300 K, where insets are snapshots of monolayer VOOH and CrOOH at the end of 15 ps of FPMD simulations.

interaction between the d orbitals of transition metal cations coupled through the p orbitals of oxygen anions. We predict that the magnetic easy-axis is in the 2D plane for the VOOH monolayer, indicating it as an XY magnet, while for CrOOH, the magnetic easy-axis is normal to the 2D planes. And the estimated critical temperatures T_c are 135 K and 100 K for monolayer VOOH and CrOOH. Our finding offers a prospect of developing the new 2D ferromagnets for future spintronic applications.

II. METHODS

All spin-polarized calculations were performed within the framework of density functional theory (DFT), as implemented in the Vienna *ab initio* simulation package (VASP) [34]. The projector augmented-wave potential [35,36] and generalized gradient approximation of Perdew-Burke-Ernzerhof functional [37] were used to describe the electron-ion interaction and exchange-correlation energy, respectively. To describe the strong on-site Coulomb interaction of localized d electrons of transition metals, the GGA + U method [38] was employed with the effective Hubbard U of 3.1, 3.5, 3.9, 3.4, and 6.0 eV for V, Cr, Mn, Co, and Ni atoms [39,40], respectively. In comparison, the band gaps of monolayer VOOH and CrOOH were also calculated by using Heyb-Scuseria-Ernzerhof (HSE06) hybrid functional. The energy cutoff for the plane-wave expansion was set to 500 eV, and a Γ-centered $13 \times 13 \times 1$ k-point mesh was adopted for the Brillouin zone integration. All structures were fully relaxed until the Hellmann-Feynman force on each atom was less than 0.01 eV/Å. The vacuum distance normal to the sheet was larger than 20 Å to eliminate the periodically repeated images' spurious interaction. Phonon dispersions of the monolayer TMOOHs were calculated with a $3 \times 3 \times 1$ supercell using the frozen phonon method as implemented in the PHONOPY package [41]. The thermal stability of monolayer TMOOHs was confirmed by performing FPMD simulations in the canonical ensemble with a constant temperature of 300 K and a time step of 1.5 fs for more than 15 ps. The exchange parameters are calculated by considering the nearest-neighbor and next-nearest-neighbor interaction, as implemented in the Heisenberg model using the same supercells and magnetic configurations as in a previous study [42].

III. RESULTS AND DISCUSSION

For monolayer TMOOHs, they have a triangular lattice with hydrogen atoms bonding with oxygen atoms at one side of the 1-T phase monolayer transition metal dioxides [43,44] [see Fig. 1(a)]. Each TM atom is coordinated with six oxygen atoms, forming a distorted octahedron with the point group of C_{3v}. As shown in Fig. 1(b), for the monolayer TMOOH, half of the oxygen atoms bonded with hydrogen atoms are marked as O1, while the oxygen atoms without hydrogen bonding are marked as O2. We first consider the dynamical stabilities of different monolayer TMOOHs by calculating their phonon spectra. For monolayer VOOH and CrOOH, there is no trace of imaginary frequency in the Brillouin zone apart from a small pocket near Γ point for monolayer VOOH [see Figs. 1(c) and 1(e)]. This feature appears to be common in other 2D systems [45,46]. The small imaginary frequencies originate from the numerical inaccuracy rather than the real

TABLE I. Optimized lattice constants (a), distances between adjacent V/Cr cations ($d_{\text{TM-TM}}$), the TM-O1/O2 bond length ($d_{\text{TM-O1/O2}}$), angles between adjacent cations intermediated by O1/O2 ($\theta_{\text{TM-O1/O2-M}}$) of monolayer VOOH and CrOOH.

	a(Å)/$d_{\text{TM-TM}}$(Å)	$d_{\text{TM-O1/O2}}$(Å)	$\theta_{\text{TM-O1/O2-TM}}$
VOOH	3.137	2.196/1.968	91.185/105.656
CrOOH	3.079	2.123/1.963	92.930/103.282

instability of 2D systems since the imaginary frequencies reduce with the increasing size of supercells used for the phonon spectra calculation (see Fig. S1 in the Supplemental Material [47]). On the other hand, the monolayer MnOOH, CoOOH, and NiOOH have large negative frequencies in the acoustic branches around the M and K points, as shown in Figs. S2(a) to S2(c) [47], indicating these monolayers are dynamically unstable. In addition, the partial density of states of phonon spectra are also shown in Fig. S2 [47]. Furthermore, the thermal stabilities of monolayer VOOH and CrOOH at room temperature are also verified by FPMD simulations [see Figs. 1(d) and 1(f)]. We thus conclude that the monolayer VOOH and CrOOH can exist as free-standing 2D structures as well as the monolayer FeOOH. In the following, we will focus on the stable monolayer VOOH and CrOOH, and their optimized structural parameters are shown in Table I.

After confirming the stabilities of the monolayer VOOH and CrOOH, we turn our attention to the magnetic properties of monolayer VOOH and CrOOH. To obtain the most stable magnetic ground states, we consider three spin configurations, i.e., FM, stripe AFM (sAFM), and zigzag AFM (zAFM) orderings as shown in Fig. 1(a), in which the supercells used are marked by dashed rectangular boxes. The results of the DFT calculations are shown in Table II. For monolayer VOOH and CrOOH, the total energies of FM configuration are lower than s/z AFM configurations. Therefore, monolayer VOOH and CrOOH all prefer an FM ground state with the magnetic moments of 2 μ_{B} and 3 μ_{B} localized at V and Cr atoms, respectively. The strength of magnetic interaction can be estimated from the relative total energies between the FM and AFM configurations [48]. Obviously, CrOOH possesses a more considerable exchange energy than VOOH, which indicates that the FM interaction in monolayer CrOOH is stronger than in monolayer VOOH (see Table II). Moreover, monolayer VOOH and CrOOH are both semiconductors with the band gap of 0.02 and 0.80 eV, respectively, by using GGA + U method as shown in Fig. S3 [47]. The band gaps obtained by using HSE06 functional are 1.8 eV and 2.3 eV, respectively, as shown in Fig. S4 [47]. Figure 2 shows the total density of states (TDOS) and partial density of states (PDOS), and the corresponding band structures and partial bands are shown in Fig. S3 [47]. It is noteworthy that, for monolayer VOOH or CrOOH, the states around the Fermi level are contributed mostly from the spin-up d electrons of V or Cr cations and slightly from the spin-up p electrons of O2 atoms.

TABLE II. Relative total energies between FM and z/sAFM configurations per unit cell ($\Delta E_z = E_{\text{FM}} - E_{\text{zAFM}}$, $\Delta E_s = E_{\text{FM}} - E_{\text{sAFM}}$), magnetic moments ($M$) of TM cations, and critical temperatures (T_{C}) for monolayer VOOH and CrOOH.

	ΔE_z(meV/f.u.)	ΔE_s(meV/f.u.)	$M(\mu_{\text{B}})$	$T_{\text{C}}(K)$
VOOH	−16.2	−15.0	2	135
CrOOH	−31.1	−31.0	3	100

To elucidate the origin of the exceptional long-range FM ordering in monolayer VOOH and CrOOH, we investigate the occupancy configuration of TM-d electrons and the interactions between TM atoms and around O atoms in these monolayers. In monolayer TMOOHs, there are six oxygen atoms around the TM atoms forming the local C_{3v} crystal field. This crystal field splits the degeneracy of TM-d orbitals into double-degenerated $e_1(e_{a1}, e_{b1})$ states, a_1 state, and double-degenerated $e_2(e_{a2}, e_{b2})$ states [49]. The corresponding wave functions derived from crystal field theory [47,49–51] for these states can be written in the form

$$\begin{aligned} e_{a1} &= \alpha_1 d_{x^2-y^2} - \beta_1 d_{xz} + \gamma_1 d_{xy} + \delta_1 d_{yz}, \\ e_{b1} &= \alpha_1 d_{xy} + \beta_1 d_{yz} - \gamma_1 d_{x^2-y^2} + \delta_1 d_{xz}, \\ a_1 &= d_{z^2}, \\ e_{a2} &= \alpha_2 d_{x^2-y^2} + \beta_2 d_{xz} + \gamma_2 d_{xy} - \delta_2 d_{yz}, \\ e_{b2} &= -\alpha_2 d_{xy} + \beta_2 d_{yz} + \gamma_2 d_{x^2-y^2} + \delta_2 d_{xz}, \end{aligned} \tag{1}$$

where β/α equals δ/γ ($\beta/\alpha > 1$ for e_1 and $\beta/\alpha < 1$ for e_2), and the coefficients derived from DFT results are listed in Table III. We find that the TM-a_1 orbital is analogous to the TM-d_{z^2} orbitals, with its z-axis directed along the crystal's c axis, and the TM-e_1 and TM-e_2 orbitals are the linear combinations of the remaining four TM-d orbitals ($d_{x^2-y^2}$, d_{xy}, d_{xz}, and d_{yz}) in the coordinates as shown in Fig. 3(a). The e_1 and e_2 orbitals at Γ point obey the symmetry of E representation in C_{3v} point group [52]. In monolayer TMOOH, the TM-e_2 orbitals have higher energy than the TM-e_1 orbitals because the e_2 orbitals point directly at six surrounding oxygen atoms. In comparison, the e_1 orbitals point between the six oxygen atoms [the pointed direction of e_1 orbitals can be viewed as the e_2 orbitals rotates 180° along the z-axis, as shown in Fig. 3(b)]. Additionally, the V(Cr) cation has a localized net magnetic moment of 2(3) μ_{B}, and consequently, V(Cr) cation has a $3d^2(3d^3)$ configuration with the valence state of $V^{3+}(Cr^{3+})$. Therefore, for monolayer VOOH, the spin-up double-degenerated states e_1 (e_{a1}, e_{b1}) are occupied, which lie in the energy range from −2 to 0 eV with reference to the Fermi level as shown in Fig. 2(b). However, for monolayer CrOOH, an extra spin-up state a_1 is occupied as well as the spin-up double-degenerated states e_1. Figure 2(e) shows that both a_1 and e_1 states lie within a 2-eV energy gap below the Fermi level.

Following the Goodenough-Kanamori-Anderson (GKA) rule [53–55], the FM coupling between the TM cations comes from the TM-O-TM superexchange interaction, and the concrete superexchange interaction could be speculated from the hybridization between TM-d orbitals and O-p orbitals according to the density of states around the Fermi level as shown in Fig. 2. For monolayer VOOH and CrOOH, there are two kinds of oxygen atoms, i.e., the O1 and O2 atoms. The bond length of TM-O1 is larger than that of TM-O2

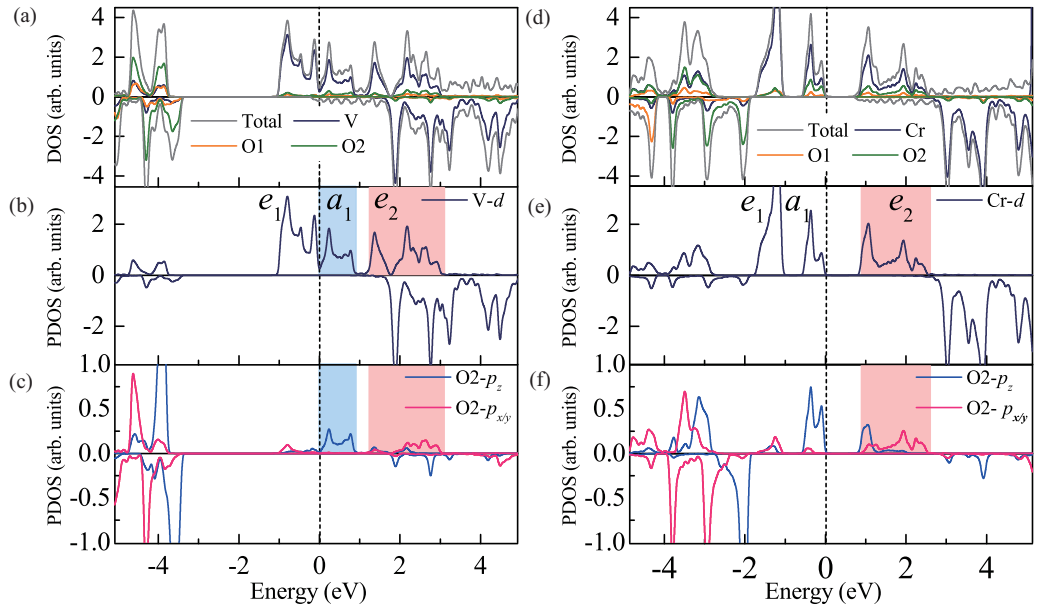

FIG. 2. (a) Total density of states (TDOS) and atomic projected density of states (PDOS) of monolayer VOOH. Orbital PDOS of (b) V-*d* and (c) O2-*p* orbitals of monolayer VOOH. (d) TDOS and atomic PDOS of monolayer CrOOH. Orbital PDOS of (e) Cr-*d* and (f) O2-*p* orbitals of monolayer CrOOH. The blue and pink shadows represent the hybridization between TM-*d* and O2-*p* orbitals. Fermi level is set at zero energy.

(see Table I), indicating the bonding of TM-O2 is stronger than that of TM-O1. Therefore, the O2-*p* orbitals play a dominant role in intermediating the TM 3*d* orbitals' superexchange interaction. Accordingly, for monolayer VOOH and CrOOH, the TM-O2-TM bond angles are all close to 90° (see Table I), which indeed favor FM ordering induced by superexchange interactions [53]. For both monolayer VOOH and CrOOH, there exists $pd\sigma$ hybridization between $p_{x/y}$ and unoccupied TM-e_2, as shown in Figs. 2(b) and 2(c) and Figs. 2(e) and 2(f). Based on the orbital symmetry, the covalent bond between $e_{a2}(e_{b2})$ orbital of TM1(TM2) and $p_x(p_y)$ orbital of O2 can form [see Fig. 3(d)], and the charge transfer occurs from the $p_x(p_y)$ orbital of O2 to the $e_{a2}(e_{b2})$ orbital of TM1(TM2), as shown by the red dotted arrow in Figs. 3(e) and 3(f). Following the Aufbau principle, the remaining p_x and p_y electrons of O2 will form triple, benefitting the FM coupling of TM cations in both monolayer VOOH and CrOOH. This superexchange interaction between TM cations intermediated by nonmetallic anions has been observed in many other 2D magnetic materials, such as $Cr_2Ge_2Te_6$ [56], TM halides [57,58], and TM sulfides [59]. However, for VOOH, extra $pd\sigma$ hybridization between O2-p_z orbital and unoccupied V-a_1 orbital is shown in Figs. 2(b) and 2(c). Based on the orbital symmetry between V-a_1 and O2-p_z orbitals, the a_1 orbitals of two nearest-neighboring V cations can interact with the same O2-p_z orbital simultaneously, according to Slater and Koster's integral formula [60], as shown in Figs. 3(c) and 3(e). Such coupling leads to an AFM coupling of V cations for

TABLE III. Coefficients of e_1 and e_2 orbitals derived from DFT results according to Eq. (1).

	α_1	β_1	γ_1	δ_1	α_2	β_2	γ_2	δ_2
VOOH	0.117	0.454	0.221	0.855	0.352	0.183	0.814	0.424
CrOOH	0.063	0.687	0.066	0.720	0.496	0.365	0.634	0.467

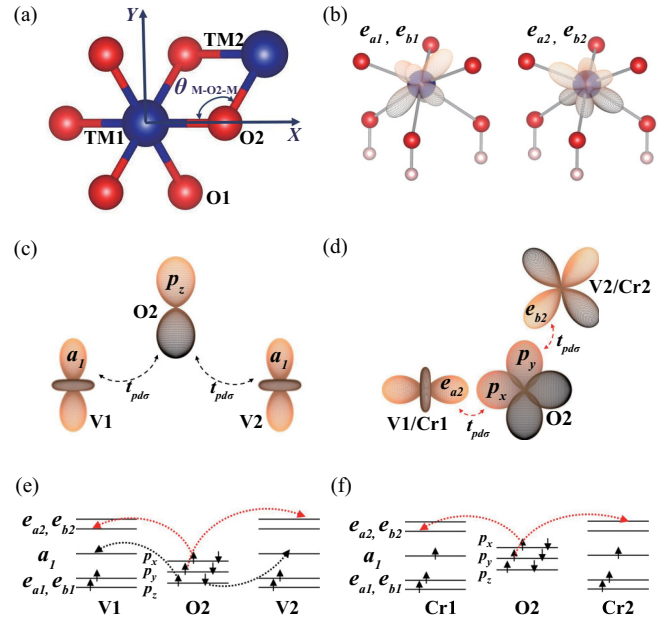

FIG. 3. (a) Set of *XYZ* coordinates in the monolayer TMOOH. (b) Schematic plot of e_1 and e_2 orbitals derived from Eq. (1). Schematic plot of the hopping channel involved in the (c) AFM superexchange: a_1-p_z-a_1 and (d) (near-) 90° FM superexchange: e_{a2}-(p_x, p_y)-e_{b2}. Virtual hopping between *d* orbitals of TM cations intermediated by O2-*p* orbitals in monolayer (e) VOOH and (f) CrOOH where red and black dashed lines represent ferromagnetic and antiferromagnetic coupling, respectively.

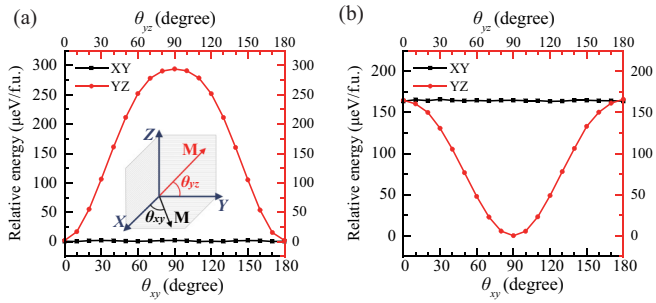

FIG. 4. Relative energy of monolayer (a) VOOH and (b) CrOOH with the magnetization rotated in XY (black line) and YZ planes (red line), with reference to the global minimum of energy.

monolayer VOOH to compete with FM coupling discussed above, resulting in a weaker FM ordering than monolayer CrOOH. In addition, the distance between two nearest-neighboring TM cations (see Table I) is much larger than that in the bulk V(Cr) metal of 2.59(2.49) Å. Therefore the direct AFM exchange between these TM cations becomes rather weak.

The uniaxial magnetocrystalline anisotropy could break the continuous symmetry and suppress the thermal agitation to stabilize the long-range FM ordering in 2D magnetic materials [16–18,25]. The MAE, determining the difficulty of spin flipping, is defined as the required energy to rotate the magnetization from the easy axis to the hard axis. To determine the MAE of monolayer VOOH and CrOOH, we calculate the total energies of the materials as a function of the rotation angle of the magnetization in XY and YZ planes, as shown in Fig. 4. The spin-orbit coupling (SOC) is included in all energy calculations. For these two monolayers, the energy is almost independent of the rotation angel θ_{xy} with the magnetization in the XY plane. However, for monolayer VOOH, the energy first increases and decreases as the rotation angle θ_{yz} with the magnetization in the YZ plane. Therefore, the monolayer VOOH can be viewed as the XY magnet [9] with a large MAE of 294 μeV/f.u., similar to VS_2 [61] and VSe_2 [62] 2D magnets. On the contrary, the energy of monolayer CrOOH reaches its minimum when the magnetization is rotated by 90° in the YZ plane, which implies that the magnetization of monolayer CrOOH along the z-axis is energetically favorable with the MAE of 165 μeV/f.u., similar to Fe_3GeTe_2 [18] and CrI_3 [17] 2D magnets.

As van Vleck proposed, SOC plays a crucial role in determining MAE [63]. To figure out how the configuration of d electrons of TM atoms influences the MAE, we use the second-order perturbation method [44,64] to analyze the MAE contribution from the electronic states around the Fermi level. Based on this theory, the MAE can be expressed as

$$\begin{aligned}\mathrm{MAE} &= \sum_{\sigma\sigma'} E^{\sigma\sigma'}(x) - E^{\sigma\sigma'}(z) \\ &= \sum_{\sigma\sigma'} (2\delta_{\sigma\sigma'} - 1)\xi^2 \sum_{o^\sigma, u^{\sigma'}} \frac{|\langle o^\sigma | L_z | u^{\sigma'} \rangle|^2 - |\langle o^\sigma | L_x | u^{\sigma'} \rangle|^2}{E_u^{\sigma'} - E_o^\sigma},\end{aligned} \tag{2}$$

where $E_u^{\sigma'}$ and E_o^σ are energy levels of unoccupied states with spin $\sigma'(|u^{\sigma'}\rangle)$ and occupied states with spin $\sigma(\langle o^\sigma|)$, respectively, ξ is the strength of SOC, and L_x and L_z are angular momentum operators. Here, the orthogonal magnetization directions, x- and z-axes, follow the coordinates in Fig. 3(a), and the positive (negative) sign of MAE suggests that the magnetization of the easy axis is along the direction of the z-axis (XY plane). For the same spin channel, the nonzero matrix elements of L_x and L_z operators contributed from d states are $\langle xz|L_z|yz\rangle = 1$, $\langle x^2 - y^2|L_z|xy\rangle = 2$, $\langle z^2|L_x|yz\rangle = \sqrt{3}$, $\langle xy|L_x|xz\rangle = 1$, and $\langle x^2 - y^2|L_x|yz\rangle = 1$. Considering that the states around the Fermi level are contributed mostly from the spin-up d electrons for monolayer VOOH and CrOOH, we can estimate the nonzero contribution between unoccupied and occupied spin-up d states around the Fermi level.

For monolayer VOOH with $3d^2$ configuration of V^{3+}, d states around Fermi level are mainly the occupied e_1 states and the unoccupied a_1 states with the same spin-up channel [see Fig. 2(b)]. Based on second-perturbation theory, the main nonzero contribution to MAE from SOC is the coupling between occupied spin-up e_1 state and unoccupied spin-up a_1 state ($|\langle e_1|L_z|a_1\rangle|^2 - |\langle e_1|L_x|a_1\rangle|^2$), which makes a large negative contribution and gives rise to the magnetization of the easy axis in XY plane for monolayer VOOH. However, for monolayer CrOOH with $3d^3$ configuration of Cr^{3+}, the MAE in Eq. (2) contains two terms where occupied states are e_1 and a_1 spin-up states and unoccupied states are only e_2 spin-up states [see Fig. 2(e)]. Although the coupling between occupied a_1 state and unoccupied e_2 state ($|\langle a_1|L_z|e_2\rangle|^2 - |\langle a_1|L_x|e_2\rangle|^2$) makes a negative contribution to the MAE, the coupling between the occupied e_1 state and unoccupied e_2 state ($|\langle e_1|L_z|e_2\rangle|^2 - |\langle e_1|L_x|e_2\rangle|^2$) makes a positive contribution and turns the MAE to be positive, resulting in the magnetization along the z-axis for monolayer CrOOH.

Finally, we estimate the critical temperature T_c for monolayer VOOH and CrOOH, where magnetic phase transition occurs. The calculated exchange parameters show that the nearest-neighbor parameter J_1 is significantly larger than the next-nearest-neighbor exchange parameter J_2 [47], so the Curie temperature T_C is determined mainly by the nearest-neighbor parameter J_1. For monolayer VOOH with the magnetization in the XY plane, as an XY magnet, there is quasi-long-range FM ordering at low temperature [9,62]. Its critical temperature in 2D triangular lattice could be estimated by $T_c = 1.335J_1/k_B$ [42,47]. The critical temperature T_c of quasi-long-range FM ordering is 135 K for monolayer VOOH. For monolayer CrOOH with the magnetization along the z-axis, the critical temperature can be estimated from the Weiss molecular field theory [47,65–67], which is 100 K.

IV. CONCLUSION

In summary, we computationally predicted the single-layer ferromagnetic semiconductors VOOH and CrOOH with excellent thermal and dynamical stabilities. The ferromagnetic ground state is stabilized by the superexchange interaction between adjacent transition metal atoms

intermediated by nearest-neighboring oxygen atoms. The MAE calculation with SOC shows that monolayer VOOH possesses the in-plane magnetization. The MAE is 294 μeV/f.u., and the critical temperature of the phase transition is determined to be 135 K. On the contrary, monolayer CrOOH is demonstrated to exhibit perpendicular magnetic anisotropy with the long-range ferromagnetic ordering stabilized by the MAE of 165 μeV/f.u.. Nevertheless, the critical temperature is around 100 K estimated from the Weiss molecular field theory. Our study demonstrates 2D intrinsic ferromagnets from transition metal oxyhydroxides for the first time and offers new 2D materials for future spintronics devices.

ACKNOWLEDGMENTS

This work was supported by the National Natural Science Foundation of China (Grant No. 11874036), Local Innovative and Research Teams Project of Guangdong Pearl River Talents Program (2017BT01N111), Science and Technology Planning Project of Guangdong Province (2020B1212060015), and Shenzhen Basic Research Project (JCYJ20200109142816479). P.T. acknowledges the support from the Fundamental Research Funds for the Central Universities (ZG216S20A1) and the 111 Project (B17002). This research was supported by the high performance computing (HPC) resources at Beihang University.

[1] K. S. Burch, D. Mandrus, and J. G. Park, Nature (London) **563**, 47 (2018).
[2] C. Gong and X. Zhang, Science **363**, eaav4450 (2019).
[3] Y. Zhu, X. Kong, T. D. Rhone, and H. Guo, Phys. Rev. Mater. **2**, 081001(R) (2018).
[4] M. Ashton, J. Paul, S. B. Sinnott, and R. G. Hennig, Phys. Rev. Lett. **118**, 106101 (2017).
[5] H. Deng, Z. Chen, A. Wołoś, M. Konczykowski, K. Sobczak, J. Sitnicka, I. V. Fedorchenko, J. Borysiuk, T. Heider, Ł. Pluciński, K. Park, A. B. Georgescu, J. Cano, and L. Krusin-Elbaum, Nat. Phys. **17**, 36 (2021).
[6] Y. Deng, Y. Yu, M. Z. Shi, Z. Guo, Z. Xu, J. Wang, X. H. Chen, and Y. Zhang, Science **367**, 895 (2020).
[7] S. Qi, R. Gao, M. Chang, Y. Han, and Z. Qiao, Phys. Rev. B **101**, 014423 (2020).
[8] V. L. Berezinskii, Sov. Phys. JETP **32**, 493 (1971).
[9] J. M. Kosterlitz and D. J. Thouless, J. Phys. C: Solid State Phys. **6**, 1181 (1973).
[10] M. Yang, Q. Li, R. V. Chopdekar, R. Dhall, J. Turner, J. D. Carlström, C. Ophus, C. Klewe, P. Shafer, A. T. N'Diaye, J. W. Choi, G. Chen, Y. Z. Wu, C. Hwang, F. Wang, and Z. Q. Qiu, Sci. Adv. **6**, eabb5157 (2020).
[11] B. Ding, Z. Li, G. Xu, H. Li, Z. Hou, E. Liu, X. Xi, F. Xu, Y. Yao, and W. Wang, Nano Lett. **20**, 868 (2020).
[12] V. K. Gudelli and G.-Y. Guo, New J. Phys. **21**, 053012 (2019).
[13] M. Wu, Z. Li, T. Cao, and S. G. Louie, Nat. Commun. **10**, 2371 (2019).
[14] W. Jin, H. H. Kim, Z. Ye, G. Ye, L. Rojas, X. Luo, B. Yang, F. Yin, J. S. A. Horng, S. Tian, Y. Fu, G. Xu, H. Deng, H. Lei, A. W. Tsen, K. Sun, R. He, and L. Zhao, Nat. Commun. **11**, 4780 (2020).
[15] N. D. Mermin and H. Wagner, Phys. Rev. Lett. **17**, 1133 (1966).
[16] C. Gong, L. Li, Z. Li, H. Ji, A. Stern, Y. Xia, T. Cao, W. Bao, C. Wang, Y. Wang, Z. Q. Qiu, R. J. Cava, S. G. Louie, J. Xia, and X. Zhang, Nature (London) **546**, 265 (2017).
[17] B. Huang, G. Clark, E. Navarro-Moratalla, D. R. Klein, R. Cheng, K. L. Seyler, D. Zhong, E. Schmidgall, M. A. McGuire, D. H. Cobden, W. Yao, D. Xiao, P. Jarillo-Herrero, and X. Xu, Nature (London) **546**, 270 (2017).
[18] Z. Fei, B. Huang, P. Malinowski, W. Wang, T. Song, J. Sanchez, W. Yao, D. Xiao, X. Zhu, A. F. May, W. Wu, D. H. Cobden, J.-H. Chu, and X. Xu, Nat. Mater. **17**, 778 (2018).
[19] S. Zhang, R. Xu, N. Luo, and X. Zou, Nanoscale **13**, 1398 (2021).
[20] H. Komatsu, Y. Nonomura, and M. Nishino, Phys. Rev. B **100**, 094407 (2019).
[21] B. Huang, G. Clark, D. R. Klein, D. MacNeill, E. Navarro-Moratalla, K. L. Seyler, N. Wilson, M. A. McGuire, D. H. Cobden, D. Xiao, W. Yao, P. Jarillo-Herrero, and X. Xu, Nat. Nanotechnol. **13**, 544 (2018).
[22] Y. Deng, Y. Yu, Y. Song, J. Zhang, N. Z. Wang, Z. Sun, Y. Yi, Y. Z. Wu, S. Wu, J. Zhu, J. Wang, X. H. Chen, and Y. Zhang, Nature (London) **563**, 94 (2018).
[23] S. Jiang, L. Li, Z. Wang, K. F. Mak, and J. Shan, Nat. Nanotechnol. **13**, 549 (2018).
[24] Y. Sun, R. C. Xiao, G. T. Lin, R. R. Zhang, L. S. Ling, Z. W. Ma, X. Luo, W. J. Lu, Y. P. Sun, and Z. G. Sheng, Appl. Phys. Lett. **112**, 072409 (2018).
[25] Ø. Johansen, V. Risinggård, A. Sudbø, J. Linder, and A. Brataas, Phys. Rev. Lett. **122**, 217203 (2019).
[26] B. Zhang, X. L. Zheng, O. Voznyy, R. Comin, M. Bajdich, M. Garcia-Melchor, L. L. Han, J. X. Xu, M. Liu, L. R. Zheng, F. P. G. de Arquer, C. T. Dinh, F. J. Fan, M. J. Yuan, E. Yassitepe, N. Chen, T. Regier, P. F. Liu, Y. H. Li, P. De Luna, A. Janmohamed, H. L. Xin, H. Yang, A. Vojvodic, and E H. Sargent, Science **352**, 333 (2016).
[27] Z. F. Huang, J. J. Song, Y. H. Du, S. B. Xi, S. Dou, J. M. V. Nsanzimana, C. Wang, Z. C. J. Xu, and X. Wang, Nat. Energy **4**, 329 (2019).
[28] J. H. Huang, J. T. Chen, T. Yao, J. F. He, S. Jiang, Z. H. Sun, Q. H. Liu, W. R. Cheng, F. C. Hu, Y. Jiang, Z. Y. Pan, and S. Q. Wei, Angew. Chem. Int. Ed. **54**, 8722 (2015).
[29] Y. M. Sun, S. N. Sun, H. T. Yang, S. B. Xi, J. Gracia, and Z. C. J. Xu, Adv. Mater. **32**, 2003297 (2020).
[30] P. N. Bityutskii and V. I. Khitrova, J. Struct. Chem. **9**, 921 (1969).
[31] M. Ichikawa, T. Gustafsson, I. Olovsson, and T. Tsuchida, J. Phys. Chem. Solids **60**, 1875 (1999).
[32] P. Chen, K. Xu, X. Li, Y. Guo, D. Zhou, J. Zhao, X. Wu, C. Wu, and Y. Xie, Chem. Sci. **5**, 2251 (2014).
[33] I. Khan, A. Hashmi, M. U. Farooq, and J. Hong, ACS Appl. Mater. Interfaces **9**, 35368 (2017).
[34] G. Kresse and J. Furthmüller, Phys. Rev. B **54**, 11169 (1996).
[35] G. Kresse and D. Joubert, Phys. Rev. B **59**, 1758 (1999).
[36] D. Hobbs, G. Kresse, and J. Hafner, Phys. Rev. B **62**, 11556 (2000).
[37] J. P. Perdew, K. Burke, and M. Ernzerhof, Phys. Rev. Lett. **77**, 3865 (1996).

[38] S. L. Dudarev, G. A. Botton, S. Y. Savrasov, C. J. Humphreys, and A. P. Sutton, Phys. Rev. B **57**, 1505 (1998).
[39] L. Wang, T. Maxisch, and G. Ceder, Phys. Rev. B **73**, 195107 (2006).
[40] A. Jain, G. Hautier, S. P. Ong, C. J. Moore, C. C. Fischer, K. A. Persson, and G. Ceder, Phys. Rev. B **84**, 045115 (2011).
[41] A. Togo and I. Tanaka, Scr. Mater. **108**, 1 (2015).
[42] S. Zhang, R. Xu, W. Duan, and X. Zou, Adv. Funct. Mater. **29**, 1808380 (2019).
[43] M. Kan, J. Zhou, Q. Sun, Y. Kawazoe, and P. Jena, J. Phys. Chem. Lett. **4**, 3382 (2013).
[44] Y. Wang, F. Li, H. Zheng, X. Han, and Y. Yan, Phys. Chem. Chem. Phys. **20**, 28162 (2018).
[45] V. Zólyomi, N. D. Drummond, and V. I. Fal'ko, Phys. Rev. B **89**, 205416 (2014).
[46] B. Özdamar, G. Özbal, M. N. Çınar, K. Sevim, G. Kurt, B. Kaya, and H. Sevinçli, Phys. Rev. B **98**, 045431 (2018).
[47] See Supplemental Material at http://link.aps.org/supplemental/10.1103/PhysRevB.103.195402 for supplementary notes, Figs. S1-S6, and Table S1, which include Refs. [42,49–51,65–67].
[48] A. S. Botana and M. R. Norman, Phys. Rev. Mater. **3**, 044001 (2019).
[49] C. Bradley and A. Cracknall, *The Mathematical Theory of Symmetry in Solids: Representation Theory for Point Groups and Space Groups* (Clarendon, Oxford, 1972).
[50] J. S. Griffith, *The Theory of Transition-Metal Ions* (Cambridge University Press, Cambridge, England, 1964).
[51] S. Jiang, *The Theory of Ferromagnetism* (Science Press, Beijing, 1993).
[52] J. Kuneš, H. Rosner, D. Kasinathan, C. O. Rodriguez, and W. E. Pickett, Phys. Rev. B **68**, 115101 (2003).
[53] J. B. Goodenough, Phys. Rev. **100**, 564 (1955).
[54] J. Kanamori, J. Phys. Chem. Solids **10**, 87 (1959).
[55] P. W. Anderson, Phys. Rev. **115**, 2 (1959).
[56] M. D. Watson, I. Marković, F. Mazzola, A. Rajan, E. A. Morales, D. M. Burn, T. Hesjedal, G. van der Laan, S. Mukherjee, T. K. Kim, C. Bigi, I. Vobornik, M. Ciomaga Hatnean, G. Balakrishnan, and P. D. C. King, Phys. Rev. B **101**, 205125 (2020).
[57] H. Wang, F. Fan, S. Zhu, and H. Wu, Europhys. Lett. **114**, 47001 (2016).
[58] V. V. Kulish and W. Huang, J. Mater. Chem. C **5**, 8734 (2017).
[59] L. Liu, I. Kankam, and H. L. Zhuang, Phys. Rev. B **98**, 205425 (2018).
[60] J. C. Slater and G. F. Koster, Phys. Rev. **94**, 1498 (1954).
[61] H. L. Zhuang and R. G. Hennig, Phys. Rev. B **93**, 054429 (2016).
[62] M. Bonilla, S. Kolekar, Y. Ma, H. C. Diaz, V. Kalappattil, R. Das, T. Eggers, H. R. Gutierrez, M.-H. Phan, and M. Batzill, Nat. Nanotechnol. **13**, 289 (2018).
[63] J. H. van Vleck, Phys. Rev. **52**, 1178 (1937).
[64] D. S. Wang, R. Wu, and A. J. Freeman, Phys. Rev. B **47**, 14932 (1993).
[65] B. D. Cullity and C. D. Graham, *Introduction to Magnetic Materials*, 2nd ed. (Wiley & Sons, Hoboken, NJ, 2009).
[66] A. R. Wildes, B. Roessli, B. Lebech, and K. W. Godfrey, J. Phys.: Condens. Matter **10**, 6417 (1998).
[67] H. L. Zhuang, Y. Xie, P. R. C. Kent, and P. Ganesh, Phys. Rev. B **92**, 035407 (2015).